The Effect of Hartree-Fock Exchange on Scaling Relations and Reaction Energetics for C–H Activation Catalysts

Vyshnavi Vennelakanti[1,2], Aditya Nandy[1,2], and Heather J. Kulik[1,*]

[1]*Department of Chemical Engineering, Massachusetts Institute of Technology, Cambridge, MA 02139*

[2]*Department of Chemistry, Massachusetts Institute of Technology, Cambridge, MA 02139*

ORCIDs:

Vyshnavi Vennelakanti: 0000-0001-7677-2902

Aditya Nandy: 0000-0001-7137-5449

Heather J. Kulik: 0000-0001-9342-0191

Acknowledgments: The authors acknowledge primary support for the catalyst design screen by the National Science Foundation under grant numbers CBET-1704266 and CBET-1846426. A.N. was partially supported by a National Science Foundation Graduate Research Fellowship under Grant #1122374. Initial conception and data set generation for this study was supported by the Department of Energy under grant number DE-SC0012702. Algorithm and workflow development as well as data collection strategies were supported by the Office of Naval Research under grant numbers N00014-17-1-2956, N00014-18-1-2434, and N00014-20-1-2150. This work was carried out in part using computational resources from the Extreme Science and Engineering Discovery Environment (XSEDE), which is supported by National Science Foundation grant number ACI-1548562. H.J.K. holds a Career Award at the Scientific Interface from the Burroughs Wellcome Fund, an AAAS Marion Milligan Mason Award, and an Alfred P. Sloan Fellowship in Chemistry, which supported this work.

ABSTRACT: High-throughput computational catalyst studies are typically carried out using density functional theory (DFT) with a single, approximate exchange-correlation functional. In open shell transition metal complexes (TMCs) that are promising for challenging reactions (e.g., C–H activation), the predictive power of DFT has been challenged, and properties are known to be strongly dependent on the admixture of Hartree-Fock (HF) exchange. We carry out a large-scale study of the effect of HF exchange on the predicted catalytic properties of over 1,200 mid-row (i.e., Cr, Mn, Fe, Co) 3*d* TMCs for direct methane-to-methanol conversion. Reaction energetic sensitivities across this set depend both on the catalytic rearrangement and ligand chemistry of the catalyst. These differences in sensitivities change both the absolute energetics predicted for a catalyst and its relative performance. Previous observations of the poor performance of global linear free energy relationships (LFERs) hold with both semi-local DFT widely employed in heterogeneous catalysis and hybrid DFT. Narrower metal/oxidation/spin-state specific LFERs perform better and are less sensitive to HF exchange than absolute reaction energetics, except in the case of some intermediate/high-spin states. Importantly, the interplay between spin-state dependent reaction energetics and exchange effects on spin-state ordering means that the choice of DFT functional strongly influences whether the minimum energy pathway is spin-conserved. Despite these caveats, LFERs involving catalysts that can be expected to have closed shell intermediates and low-spin ground states retain significant predictive power.

KEYWORDS: Density functional theory, homogeneous catalysis, C–H activation, methane conversion, mid-row transition metals, open shell transition metal catalysts

1 Introduction

Computational chemistry is an essential tool in the understanding of catalytic phenomena [1-6] and in the design of catalysts [7-14]. Nevertheless, challenges remain in realizing the goal of fully computational predictive catalyst design, primarily related to when approximations in modeling the catalytic cycle or in the electronic structure method are suitably predictive. Both fundamental studies and high-throughput screens are nearly exclusively carried out with approximate DFT using an approximate exchange-correlation functional [6,15]. For heterogeneous catalysis, the semi-local (e.g., generalized gradient approximation, GGA) DFT functionals used due to the high cost of hybrid exchange in periodic calculations introduce numerous limitations [16,17]. Conversely, using hybrids as is common in molecular catalysis[18] does not guarantee improved property prediction in molecules or in solids[19,20]. For both heterogeneous and homogenous transition metal catalysis, the well-localized (e.g., 3*d*) electrons[17,21,22] make predictions sensitive to the choice of the functional and to the chemical composition of the catalytic intermediate.

These challenges for computational catalysis arise from the approximations of practical DFT that give rise to the twin challenges of self-interaction error or delocalization error [23-26] and static correlation error that have been described as a zero sum game [27]. The errors associated with approximate DFT in turn affect the predictions of properties relevant to computational catalyst design including barrier heights [28], bond dissociation energies [29-33], magnetic moments [21,34,16,35], spin-state ordering [35-40], electron affinities [41-43], and band gaps [44,23]. It is seldom known *a priori* what the best functional is to study a particular set of catalysts due to differences in types of errors and degree of error cancellation that are known to be strongly dependent on catalyst chemistry [35,36,45,46]. While for narrow chemical

compositions, it may be possible to tailor a functional to improve errors [47] or develop an empirical correction scheme [48], this approach will fail if the exact benchmark (e.g., experimental) result is not known or when wider variations in chemistry are studied. As a result, the errors introduced by exchange-correlation approximations can strongly influence property prediction [49,30,50,26,51-53].

As an alternative, both uncertainty quantification and sensitivity analysis have been employed. For example, Bayesian inference approaches on established functionals [54-56] or in an ensemble of designed functionals [57] have been developed to estimate uncertainty in DFT predictions for heterogeneous catalysis [58-60], adsorption energies [61], and magnetic ground states [62]. Sensitivity analysis has also been fruitfully employed for understanding sensitivity to exchange-correlation functional [45,63-65]. For molecular open shell transition metal complex (TMC) catalysts in particular, predictions are known to be strongly sensitive to the degree of Hartree-Fock (HF) exchange [39,38,35,63,36]. Predicted properties typically vary linearly with admixture of HF exchange, making the evaluation of linearized sensitivities valuable in assessing property sensitivity to functional choice [36,66,63,35,67]. This sensitivity analysis has uncovered paradoxical behaviors: while HF exchange is expected to increase barrier heights, recent studies have revealed it can also paradoxically reduce barrier heights in TMCs [65,63] in a manner that has been rationalized in terms of delocalization imbalances between reactants and transition states [45].

Within computational catalysis, linear free energy relationships (LFERs) are also an expedient, widely used approximation. For example, design of catalysts capable of selective partial oxidation[68-76] has been shown [77] to be limited in heterogeneous catalysis by a strong scaling relationship between the formation of a reactive metal-oxo intermediate and the

abstraction of a hydrogen atom from a substrate by the metal-oxo. In addition to reducing the number of DFT calculations required by relating catalyst activity to a single descriptor, LFERs have also been shown to less sensitive to functional choice than property prediction [78-80]. While LFERs are most widely exploited to understand catalyst design limitations in heterogeneous catalysis (e.g., for C-H activation [77,81,82]), others have shown they hold in some single-site [83] and homogeneous catalysts [84-86]. Nevertheless, the structural flexibility and variability afforded by single metal sites in homogeneous TMCs with open-shell metals has suggested LFER applicability is more limited here [87,88,14,89,90]. Compounding the challenges with interpreting these two competing effects is the extent to which these observations could be sensitive to the choice of DFT functional employed in the studies, i.e., GGAs for heterogeneous catalysis or hybrids for the molecular studies.

For catalysis with a single metal site, a closely related concern is the extent to which HF exchange is known to strongly influence the ground state spin. Indeed, when multiple spin states are known to be favored by a catalyst [91-94], this can affect fundamental aspects of the potential energy surface [95], catalyst kinetics [96], and mechanism [97]. Two state reactivity (TSR) [98-100,91] is a fundamental model that has been invoked to explain experimental observations of sluggish kinetics in reactions with conserved spin in intermediates. In TSR, it is proposed that interconversion between spin states to an excited state with shallow energy barriers occurs during catalysis. These observations motivate a better understanding spin-state specific reaction barriers for the modeling and design of open-shell TMC catalysts. Nevertheless, this is particularly challenging for approximate DFT, as GGAs tend to over-stabilize low spin states while hybrid functionals tend to over-stabilize high spin states [21,63,35,16,34]. Thus, slight adjustments to the choice of DFT functional could be expected to simultaneously change both

the ground state spin and reactivity within a spin state.

In this work, we identify and quantify the limitations of choosing a single DFT functional while carrying out large-scale screening for catalyst discovery. By employing a data set of over 1,200 catalyst compositions with numerous open shell metals in multiple spin and oxidation states, we also determine the extent to which observations are strongly sensitive to the size and diversity of the data set employed. We discuss which observations of catalyst performance, the presence and nature of LFERs, as well as spin-state-dependent reactivity are sensitive to both of these factors in computational catalyst design. Finally, we conclude with recommendations regarding computational catalyst design strategies that will be robust within the limitations of using a single, approximate DFT functional.

2 Reaction Mechanism

In this work, we extend upon a previously curated [88] set of candidate transition metal complexes (TMCs) for catalyzing the radical rebound partial oxidation of methane-to-methanol [101,88]. We focus on the thermodynamics of a catalytic cycle that consists of four reaction steps: metal-oxo formation, hydrogen atom transfer (HAT), radical rebound, and methanol release (Fig. 1). As in prior work [88], the reaction energy for metal-oxo (**2**) formation from the resting state (**1**), ΔE(oxo), is computed with N_2O as the oxygen atom source

$$\Delta E(\text{oxo}) = E(\mathbf{2}) + E(N_2) - E(\mathbf{1}) - E(N_2O)$$

The reaction energy for the abstraction of hydrogen atom from methane to form the metal-hydroxo moiety (**3**) and methyl radical ($CH_3\cdot$), ΔE(HAT), is computed as

$$\Delta E(\text{HAT}) = E(\mathbf{3}) + E(CH_3\cdot) - E(\mathbf{2}) - E(CH_4)$$

The reaction energy for the radical rebound step, ΔE(rebound), where $CH_3\cdot$ recombines with the

metal-hydroxo moiety to form metal bound methanol (**4**) is computed as

$$\Delta E(\text{rebound}) = E(\mathbf{4}) - E(\mathbf{3}) - E(CH_3\cdot)$$

The reaction energy for methanol release that returns the catalyst to its resting state (**1**), ΔE(release), is computed as

$$\Delta E(\text{release}) = E(\mathbf{1}) + E(CH_3OH) - E(\mathbf{4})$$

At variance with prior work [88], here we compute ΔE(HAT) only with the ferromagnetically coupled hydrogen atom and ΔE(rebound) with the antiferromagnetically coupled methyl radical.

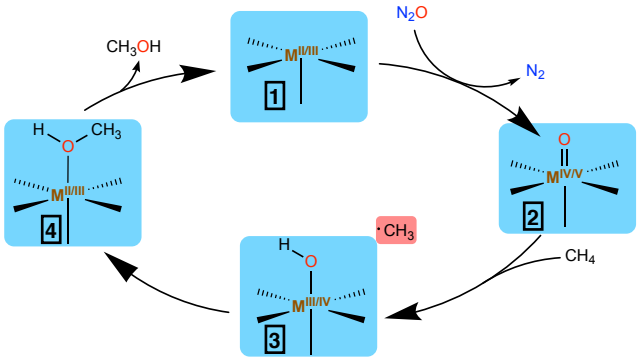

Fig. 1 Catalytic cycle for the radical rebound partial oxidation of methane-to-methanol. The cycle proceeds clockwise in four steps, starting from the resting state where the metal (M) is in oxidation state II/III. The reaction steps are: (a) Formation of metal-oxo M(IV/V)=O (**2**) from resting state M(II/III) (**1**) with N_2O oxidant, (b) hydrogen atom transfer from methanol to form metal-hydroxo M(III/IV)-OH (**3**), (c) methyl radical rebound to form a metal-bound methanol intermediate M(II/III)-CH_3OH (**4**), and (d) return to resting state M(II/III) (**1**) through methanol release. The metal (M) is shown in brown, and M=Cr, Mn, Fe, or Co in the catalysts studied in this work

3 Computational Details

The catalysts studied in this work extend upon structures curated in Ref. [88]. We briefly reiterate their structures and the procedure developed in Ref. [88] followed by the extensions or additional considerations in the current work. The present set of 1,207 mononuclear TMCs are those for which we have the converged intermediate structures and energies obtained in Ref. [88]

for the proposed reaction mechanism (see Sec. 2). These TMCs are formed with four mid-row 3*d* metals (M = Cr, Mn, Fe, Co) in M(II/III) oxidation states with total charge conserved in the catalytic cycle. We study all catalysts in up to three spin states: LS doublet for d^3 Cr(III), LS singlet and IS triplet for d^4 Cr(II)/Mn(III), LS doublet and IS quartet for d^5 Mn(II)/Fe(III) and d^7 Co(II), and LS singlet, IS triplet, and HS quintet for d^6 Fe(II)/Co(III).

As in prior work [88], all density functional theory (DFT) geometry optimizations and single point energy calculations were carried out in a developer version of TeraChem v1.9 [102]. Initial structures were generated by molSimplify [103], which uses OpenBabel [104,105] as a backend, and calculations were automated with molSimplify Automatic Design (mAD)[106] for automated resubmission and geometric health checks. In Ref. [88], all geometry optimizations used the hybrid generalized-gradient approximation (GGA) B3LYP [107-109] exchange-correlation functional and incorporated an empirical D3 dispersion [110] correction with Becke-Johnson [111] damping. All calculations employed the LACVP* composite basis set, which consists of a LANL2DZ effective core potential [112,113] for transition metals, Br, and I, and the 6-31G* basis [114] for all the other atoms. Geometry optimizations were carried out in translation rotation internal coordinates [115] using the L-BFGS algorithm with default thresholds of 4.5×10^{-4} hartree/bohr for the gradient and 1×10^{-6} hartree for changes in the self-consistent field (SCF) energy. Singlet calculations were carried out in a spin-restricted formalism while calculations with all the other spin multiplicities employed a spin-unrestricted formalism. Level shifting [116] of 0.25 Ha to all virtual orbitals was employed to aid SCF convergence to the default criterion of 3×10^{-5} for the direct inversion of the iterative subspace (DIIS) error.

In this work, we performed Hartree-Fock (HF) exchange resampling on all intermediates and catalysts from ref. [88] that already had successfully converged B3LYP optimizations. The

initial work[88] solely computed reaction thermodynamics obtained from gas phase electronic energies, neglecting vibrational and other entropic or enthalpic corrections, solvent effects, and omitting calculation of transition states, which are all conventions that we extend to the present study on the data set from prior work. The exchange-resampling procedure follows the one we established previously [117] in which we vary the HF exchange fractions (a_{HF}) from 0.00 to 0.30 in increments of 0.05 while holding the LDA/GGA exchange ratio fixed [36,46] and reoptimize the gas phase structure. As with the original calculations [88], the exchange-resampling geometry optimizations were automated with mAD [106] in 24-hour increments with resubmissions for up to five additional runs. At each exchange fraction, the structure is reoptimized starting from the geometry and converged wavefunction of the prior exchange fraction. If one a_{HF} optimization did not converge, calculations with the subsequent a_{HF} value(s) were not attempted. This procedure was also carried out for the resting state structures, which are modeled as before [11,88] as single point energy calculations on a modified metal-oxo intermediate with the oxygen atom removed. We then performed checks of the geometry [88] to evaluate the fidelity of the optimized geometry (Table S1). We also filtered calculations for significant spin contamination, as judged through deviations of the expectation of the $\hat{S}^2$ operator from its anticipated value (i.e., $S(S+1)$) greater than or equal to 1 μ_B^2. Of the 33,796 catalytic intermediates at seven exchange fractions, the vast majority (i.e., 32,243 or ca. 95%) passed both filters (Table S2).

In this work, we computed linearized exchange sensitivities obtained from linear fits of the reaction energy as a function of HF exchange for each of the four reaction energies (Fig. 1 and see Sec. 2). Sensitivities are reported as the change in energy of a reaction step per unit of HF exchange (i.e., from 0 to 100%) that we refer to as "HFX". To ensure that we obtain

quantitative linearized sensitivities, we applied a series of constraints and checks to catalysts for each reaction step (Text S1). After completing the filtering process for each individual reaction step, we performed final checks and obtain a set of 718 catalysts for which we have reaction energies for both oxo formation and HAT (Table S3). From this subset, we identified 96 catalyst compositions for which the ground state could be determined (i.e., all spin states were converged) for all intermediates involved in oxo formation and HAT (Table S4). We determined the linearized exchange sensitivities for each spin state for these relevant intermediates following the same procedure as for reaction energies. The data set of catalysts (i.e., in any spin state) for which we have all four reaction energies contains 358 catalysts (Table S5 and Fig. S1). From this set, we identified 22 catalyst compositions for which the ground state could be determined at each reaction step and HF exchange fraction (Table S6).

4 Results and Discussion

4.1 Hartree-Fock Exchange Sensitivities of Reaction Energies

While most computational screening efforts are carried out with a single functional [118,81], a prior study from our group [63] of the methane-to-methanol cycle with a model HS Fe(II) catalyst with minimal ammonia ligands aimed to understand the magnitude of the effect of Hartree-Fock (HF) exchange on reaction thermodynamics. This work indicated a divergent effect of increasing HF exchange that made ΔE(oxo) less favorable and ΔE(HAT) more favorable [63]. In recent work on a larger set of catalysts using the B3LYP functional (a_{HF} = 0.20) [88], we observed distinct reaction energetics for each step with metal, oxidation state, and spin-state, motivating us to identify the relationship between reaction energetics and choice of HF exchange fraction over this larger set.

The linearized HF exchange sensitivities for the four reaction steps in methane-to-

methanol conversion across our large (> 1200 catalyst) set reveals broad trends. We indeed observe positive HF exchange sensitivities for most Δ*E*(oxo) values in the data set, with only a small minority (ca. 1%) instead exhibiting negative sensitivities (Fig. 2). The few compounds with negative sensitivities for Δ*E*(oxo) are Co catalysts with strong field ligands (Table S7 and Fig. S2). In contrast to Δ*E*(oxo), all Δ*E*(HAT) and most Δ*E*(rebound) energetics exhibit negative HF exchange sensitivities, indicating that the Δ*E*(HAT) and Δ*E*(rebound) reaction energies become more thermodynamically favorable with an increase in HF exchange fraction (Fig. 2). The small minority (ca. 2%) of compounds that have positive Δ*E*(rebound) HF exchange sensitivities are Cr, Mn, and Co catalysts with a range of ligand field strengths (Table S8 and Fig. S3). Thus for most catalysts, increasing the HF exchange fraction will make Δ*E*(oxo) less favorable and Δ*E*(HAT) more favorable, in accordance with prior work [63]. Within the case study of a model catalyst, the effect of HF exchange on reaction energetics was attributed [63] to increased delocalization in the metal-oxo product for oxo formation compared to reduced delocalization for the metal-hydroxo bond in HAT, an effect that is likely preserved even across a large array of metals and oxidation states.

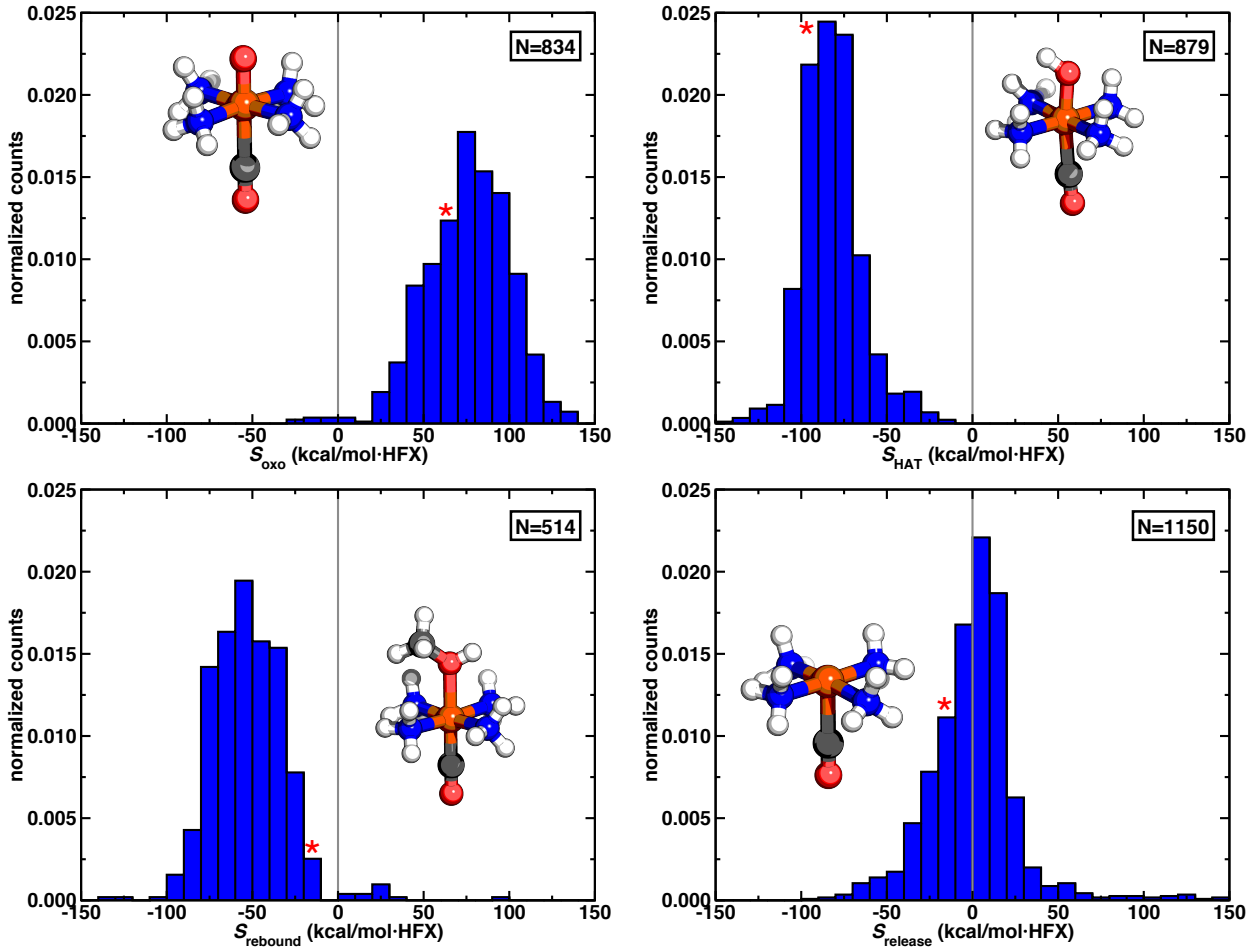

Fig. 2 Normalized histograms of sensitivities, *S* (in kcal/mol-HFX), from left to right and top to bottom: Δ*E*(oxo), Δ*E*(HAT), Δ*E*(rebound), and Δ*E*(release) reaction steps. The number of catalysts, N, for a given reaction step is indicated within the corresponding histogram. A representative catalyst, Fe(II)$(NH_3)_4$(CO), is shown in the inset with the sixth, axial catalytic moiety shown as oxo, hydroxyl, methanol, or none depending on the intermediate. A red asterisk near a bar in each pane indicates the sensitivity for the inset catalyst. Hydrogen, carbon, nitrogen, oxygen, and iron atoms are shown in white, gray, blue, red, and brown, respectively. The vertical gray line indicates a sensitivity of 0. The bin width is 10 kcal/mol·HFX

Unlike the other three steps, the HF exchange sensitivities for the methanol release step are centered near zero, with an equal balance of relatively small (< |40 kcal/mol·HFX|) positive or negative values (Fig. 2). Since most functionals used in computational screening have HF exchange fractions in the 0.00–0.25 range, this sensitivity corresponds to changing Δ*E*(release) by about 10 kcal/mol over the typical range, which is no more than around 10% of its magnitude in these catalysts [88]. To put the remaining steps in context with respect to quantities such as

spin splitting energies that are highly sensitive to exchange, the average Δ*E*(oxo) sensitivity of 75 kcal/mol·HFX and Δ*E*(HAT) sensitivity of -82 kcal/mol·HFX are both comparable to spin-splitting sensitivities [46] and to those reported previously on a model Fe(II) catalyst [63]. The spread of the distribution for Δ*E*(HAT) is narrower than for Δ*E*(oxo) (i.e., standard deviation of 17 kcal/mol·HFX vs. 24 kcal/mol·HFX for Δ*E*(oxo)), suggesting that the Δ*E*(oxo) sensitivity is likely to be more dependent on the underlying catalyst chemistry (e.g. metal, oxidation state, spin state, and ligand field). For the overall catalytic cycle, optimal functional choice and sensitivity to the HF exchange fraction in the functional is thus likely to be dominated by the dependence of the first three (i.e., oxo formation, HAT, and rebound) reaction steps. Regardless of functional choice, Δ*E*(release) nevertheless remains the thermodynamic sink of the energy landscape, despite strong functional-dependence of the other reaction steps.

Next, we quantified the origins of the underlying variations of reaction energy sensitivity distribution. We recall that for 99% of catalysts, these sensitivities range from 0 to 150 kcal/mol·HFX for oxo formation and from -150 to 0 kcal/mol·HFX for HAT and rebound reaction steps. Within these distributions, we observe limited metal-dependence of sensitivities for oxo formation and HAT reaction steps, i.e., metal-grouped mean sensitivities are comparable to the overall mean sensitivities for both Δ*E*(oxo) and Δ*E*(HAT) (Figs. 2 and 3 and Table S9 and Figs. S4–S5). For the rebound step, we instead observe moderate metal dependence, with later transition metal (e.g., Fe and Co) catalysts having more negative average sensitivities (by ca. 20-60%) compared to earlier (i.e., Cr and Mn) catalysts (Fig. 3 and Table S9 and Figs. S4–S5). While for HAT there is no apparent difference in sensitivity for M(II) vs M(III) catalysts, some dependence is observed for oxo and rebound (Fig. 3 and Table S10 and Figs. S6–S7). Specifically, the average sensitivities are larger in magnitude for oxo formation with Mn(III)

(i.e., more positive) and for rebound with Mn(III)/Fe(III) (i.e., more negative) compared to their M(II) counterparts by ca. 20 kcal/mol·HFX (Fig. 3 and Table S10 and Figs. S6–S7). Nevertheless, this trend is specific to those metals, as we observe no difference for Co(II) vs Co(III) reaction energy sensitivities for any of the reaction steps (Fig. 3 and Table S10 and Fig. S6).

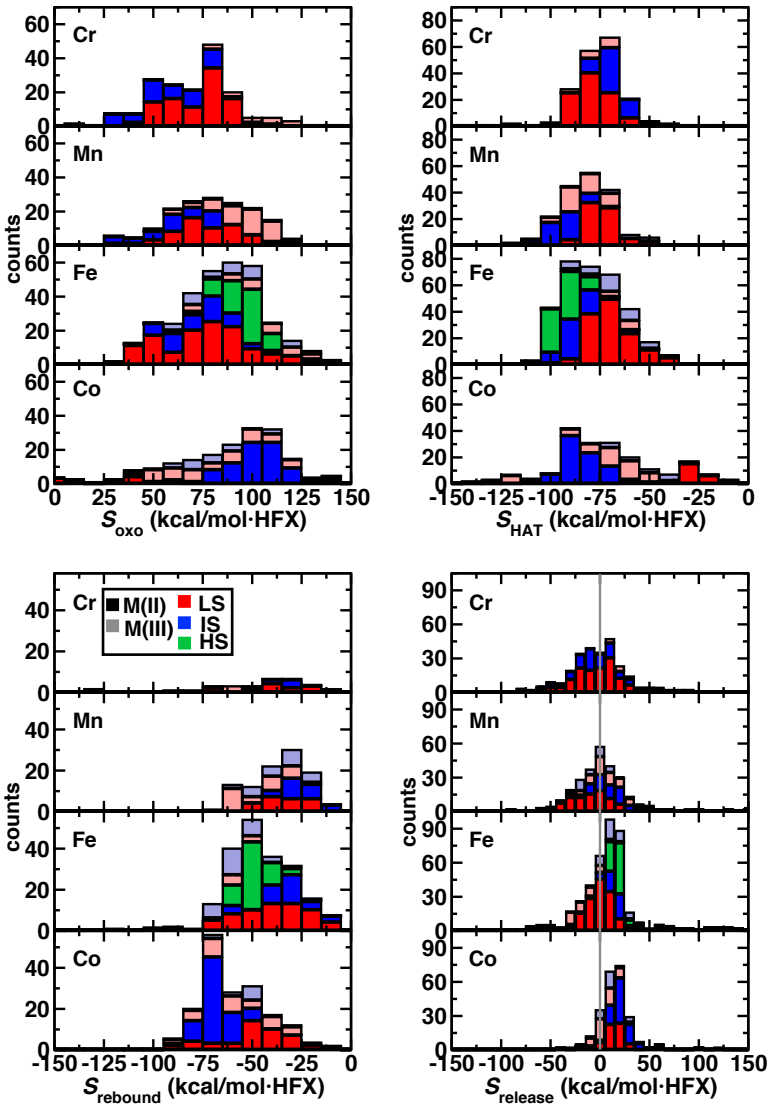

Fig. 3 Stacked histograms of sensitivities, *S* (in kcal/mol·HFX), from top to bottom and left to right: Δ*E*(oxo), Δ*E*(HAT), Δ*E*(rebound), and Δ*E*(release) reaction energies. All stacked histograms are grouped by metals Cr, Mn, Fe, and Co from top to bottom in each pane. These histograms are colored by spin state (LS in red, IS in blue, HS in green) and shaded by oxidation state (M(II) solid and M(III) translucent). The corresponding legend is in the bottom left pane. The vertical gray line indicates a sensitivity of 0 for Δ*E*(release). The bin width is 10

kcal/mol·HFX

Spin-state dependence of reaction energy exchange sensitivities is particularly concerning because the spin state can simultaneously be expected to be shifted by HF exchange. Thus, it is critical to understand if spin-state and reaction energy exchange sensitivities cooperatively amplify functional dependence of reactivity. Notably, for Fe(II) three spin states (i.e., HS, IS, and LS) are evaluated in appreciable quantities, whereas for all other combinations, only two spin states (i.e., IS and LS) were computed or limited data is available (i.e., for Co(III), see Sec. 3). We indeed observe spin-state dependence for the sensitivities in some metals/oxidation states (e.g., Mn(II/III), Fe(II), and Co(II)) but a limited effect in other (e.g., Cr(II/III), Fe(III), and Co(III)) cases (Fig. 3 and Table S11). For Mn catalysts, the spin-state dependence is significant for HAT, for example, with IS Mn(II) catalyst sensitivities more negative on average (by ca. 18 kcal/mol·HFX) than LS Mn(II) catalysts, but we observe no difference for oxo formation or rebound with these catalysts (Fig. 3 and Table S11). This effect is also not observed in the isoelectronic Fe(III) catalysts (Fig. 3 and Table S11).

Instead, Fe(II) catalysts behave similarly to Mn(II), with more positive oxo formation sensitivities and more negative HAT sensitivities (by ca. 20 kcal/mol·HFX in both cases) for the HS states with respect to LS states of the same catalyst (Fig. 3 and Table S11 and Fig. S8). Higher sensitivity of higher-spin states is most apparent in the sensitivities of oxo formation and HAT for Co(II) catalysts where the IS sensitivity is higher in magnitude than the LS one by ca. 55 kcal/mol·HFX (Fig. 3 and Table S11 and Fig. S8). Notably, the spin-state dependence of sensitivities is not obviously related to the convention of the LS state (i.e., open shell doublet vs closed shell singlet), since the spin-state-dependent Mn(II) and independent Fe(III) both have LS

doublets, whereas spin-state-dependent Fe(II) is an LS singlet.

We analyze the relationship between the Δ*E*(oxo) and Δ*E*(HAT) sensitivities to understand whether catalysts with increased positive sensitivity in Δ*E*(oxo) also have increased negative sensitivity in Δ*E*(HAT). Such a trend may be expected since the reaction energy sensitivities have been proposed to be correlated to the same measure of metal-ligand delocalization (i.e., the bond valence) [63]. Over our larger set, we find that Δ*E*(oxo) and Δ*E*(HAT) sensitivities are not necessarily correlated, implying that the knowledge of HF exchange sensitivity of Δ*E*(oxo) does not enable the prediction of sensitivity of Δ*E*(HAT). For example, two LS Fe(II) catalysts, Fe(II)$(NCS^-)_4(H_2O)$ and Fe(II)(porphyrin)(pyrrole), have different Δ*E*(oxo) sensitivities (ca. 118 and 49 kcal/mol·HFX) but have similar Δ*E*(HAT) sensitivities (ca. -80 kcal/mol·HFX, Fig. S9). On the other hand, two IS Co(III) catalysts, Co(III)$(NH_3)_4(H_2O)$ and Co(III)$(CN^-)_4(H_2O)$, have comparable Δ*E*(oxo) sensitivities ca. 80 kcal/mol·HFX but very different Δ*E*(HAT) sensitivities (-135 and -44 kcal/mol·HFX, Fig. S9). These observations are not necessarily at odds with previous observations [63] that positive sensitivities correlated to increasing delocalization and vice versa but instead suggest that changing ligand chemistry likely alters the delocalization difference in reaction steps independently. Thus, functional choice may tune the energetics for one reaction step without impacting another, and the optimal choice of functional could vary both by catalyst and reaction step.

4.2 Trends in Oxo Formation and HAT Reaction Energetics

The oxo formation and HAT steps are widely studied due to their well-known favorability trade-off [77,118,14,81,89,88] that must be optimized to design catalyst candidates

for direct methane-to-methanol conversion. Some studies have exploited scaling relations between ΔE(oxo) and ΔE(HAT) [77,118,81], whereas others have shown that they can be disrupted [14,89,88]. The first set of studies have typically been carried out with a GGA functional [81,118,77], whereas the latter set employed the GGA hybrid B3LYP (a_{HF} = 0.20) functional [88,14]. Thus, it is important to understand if trends in energetics of oxo formation and HAT reaction steps and the nature and applicability of scaling relations are dependent on HF exchange. Our analysis of sensitivities for these steps indicates that the catalysts should exhibit less favorable ΔE(oxo) and more favorable ΔE(HAT) with increasing a_{HF}. Indeed, we observe increasing a_{HF} to simultaneously shift all catalysts to less favorable ΔE(oxo) values and more favorable ΔE(HAT) values (Fig. 4). Although these absolute energies change with a_{HF}, the wide ranges of reaction energies in the ΔE(oxo) and ΔE(HAT) distributions are not significantly exchange sensitive (Fig. 4 and Figs. S10–S13). Thus, observations with hybrid DFT of limited applicability of a global scaling relationship between oxo and HAT [14,89,88] hold even at the GGA level of theory. This suggests that differences in the observed applicability of global scaling relations should be attributed more to the set of catalysts studied than the level of theory.

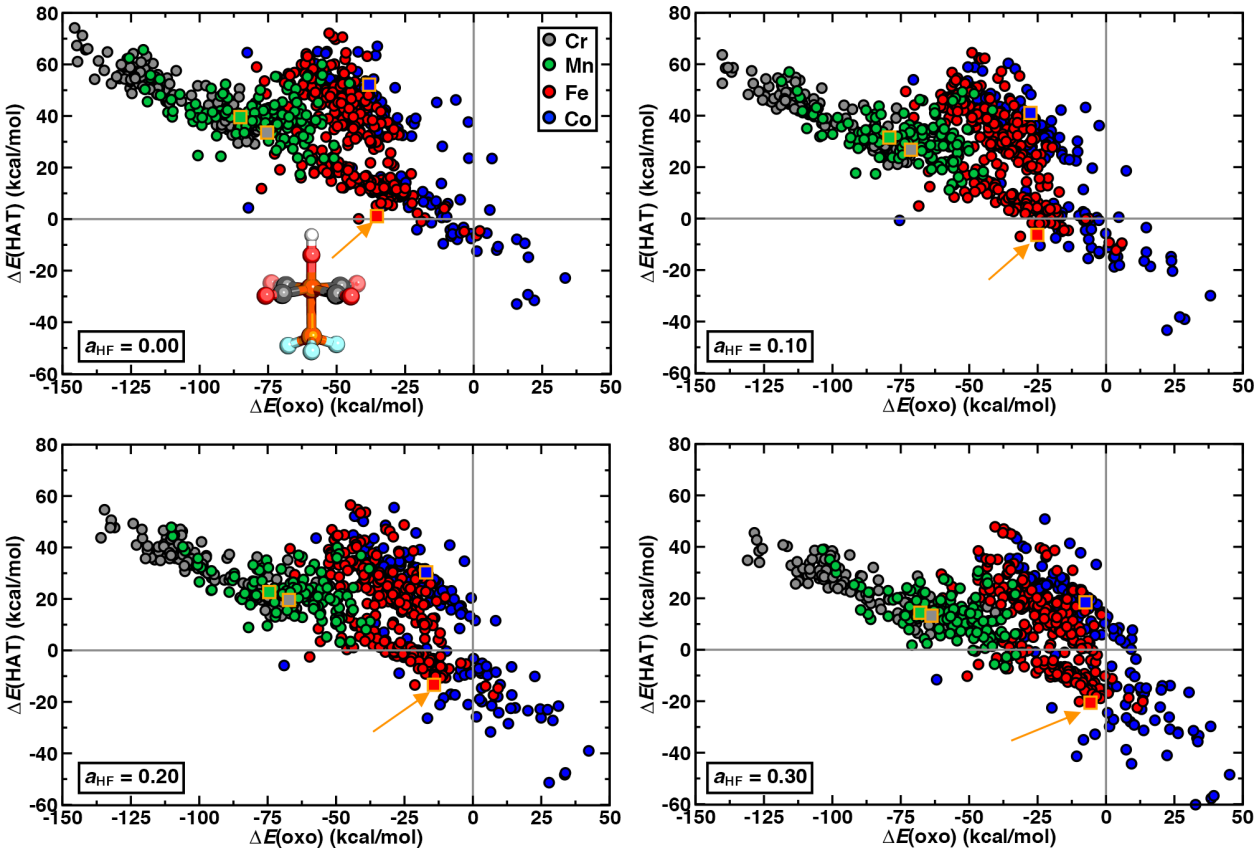

Fig. 4 ΔE(oxo) vs ΔE(HAT) reaction energies (in kcal/mol) of catalysts shown as data points colored by metal (Cr in gray, Co in blue, Fe in red, and Mn in green), as in top left inset legend. Energy landscapes in the four panes correspond to those obtained at a_{HF} = 0.00, 0.10, 0.20, and 0.30 from left to right and top to bottom, as indicated in inset. A representative catalyst for each metal center is shown as an orange outlined square to highlight how reaction energies change with change in HF exchange fraction, and one representative Fe(III) catalyst is shown with the hydroxo moiety (i.e., Fe(IV)-OH$(CO)_4(PF_3)$ in top left inset and annotated with arrows in all panes). Ball and stick structures are colored by element as: H in white, C in gray, O in red, F in cyan, P in orange, and Fe in brown. The solid gray lines represent zero-axes in all the plots

Examining trends by metal with increasing HF exchange (i.e., a_{HF} from 0.00 to 0.30), we next assessed if these global changes alter which metals are expected to have favorable reaction energetics. Early transition metal (i.e., Cr and Mn) catalysts have unfavorable ΔE(HAT) irrespective of functional choice (Fig. 4 and Tables S12–S13 and Figs. S14–S16). For later metals, more HF exchange sensitivity is apparent: for increasing a_{HF} a greater number of Fe catalysts have simultaneously exothermic ΔE(HAT) and ΔE(oxo), and more Co catalysts have

exothermic ΔE(HAT) but at the cost of increasingly endothermic ΔE(oxo) value (Fig. 4 and Tables S12–S13 and Figs. S14–S16). Thus, we would expect a GGA high-throughput screening to have a bias toward Co catalysts, whereas hybrids would favor Fe catalysts that are more consistent with general experimental observations.

We also observe the distribution of ΔE(oxo) for Cr catalysts to widen with HF exchange, while the equivalent distributions for Mn, Fe, and Co catalysts narrow (by ca. 10%, Fig. 4 and Tables S14–S15 and Figs. S17–S24). In contrast, over the same range of a_{HF}, the Cr, Mn, and Fe metals have narrowing ΔE(HAT) distributions, whereas Co widens (by ca. 11%, Fig. 4 and Tables S14–S15 and Figs. S17–S24). These differences are likely attributable to a greater heterogeneity in the degree and nature of bond delocalization in Cr catalysts for oxo formation and Co for HAT (e.g., due to differences in the nature of the metal-oxo bond [88]). Overall, the definition of what catalyst optimizes this reaction shifts only moderately with increasing a_{HF} to encompass a greater number of Fe catalysts, but the specific identities of the most favorable catalysts are likely even more sensitive to the a_{HF} value.

We return to the question of differences in the global scaling relationship (i.e., linear free energy relationship or LFER) obtained with the B3LYP hybrid [88] versus those obtained in literature data sets with GGAs [77,81]. In prior work [88], the global scaling relation obtained with B3LYP indicated a shallower trade-off between HAT and oxo compared to literature values, but a large mean absolute error of prediction for the global scaling relation over a set of over 2,000 catalysts that motivated evaluation of LFERs by metal, oxidation state, and spin state [88] with smaller errors. We now investigate how these global and metal/oxidation/spin-state-specific LFERs as well as their standard deviations change as a function of HF exchange (Table S16). Analyzing the global LFER, we observe that our slope is insensitive to a_{HF} and comparable

to the previously obtained slope (ca. -0.3 ΔE(HAT)/ΔE(oxo)), and a comparably large mean absolute error (MAE) of prediction (>10 kcal/mol) limits applicability in screening of this LFER (Table S16). The key difference with increasing a_{HF}, is that the global LFER intercept unsurprisingly decreases with increasing a_{HF} by around 16 kcal/mol, with unchanged standard deviation (Fig. S25). Given that this global scaling relation would still lack predictive power as a screening tool, we assessed whether metal and oxidation/spin-state specific LFERs are also invariant with a_{HF} (Figs. S26–S29).

To identify exchange sensitivity of these individual scaling relations, we focus on the case of Fe(II) resting state catalysts that has been computed in three spin states, i.e. LS singlet, IS triplet, or HS quintet. The Fe(II) case is also the only metal/oxidation state combination in our set for which we have computed all three spin states with appreciable data. The qualitative trend [88] with B3LYP of a shallower LS Fe(II) slope (ca. -0.3) vs HS Fe(II) (ca. -0.6) and the IS Fe(II) inbetween (ca. -0.45) approximately holds for all HF exchange fractions, but we do observe some quantitative changes (Fig. 5). The IS Fe(II) catalyst LFER is strongly functional dependent, with steeper slopes at higher a_{HF}, i.e., from around zero for a GGA to < -0.4 at a_{HF} = 0.30 (Fig. 5). The standard error on this spin state is high, highlighting limited applicability of an LFER here (Fig. 5). In comparison to the other two spin states, IS Fe(II) is seldom a ground state in a spin-conserved reaction coordinate with B3LYP [88], suggesting that LS or HS Fe(II) LFERs that are invariant or slightly sensitive to exchange could instead be used for screening (Fig. 5). From a_{HF} = 0.00 to 0.30, intercepts shift downward to varying degrees for the three spin states, with the largest (ca. 40 kcal/mol) for the IS catalysts and a smaller adjustment for HS or LS (ca. 10–15 kcal/mol) that is comparable to the observed global intercept change (Fig. 5 and Fig. S25). Although our analysis focused on Fe(II), similar observations hold true for other metal

catalysts, with the IS LFER slopes varying markedly for all metals, whereas only the intercept shifts significantly for LS states (Fig. 5 and Figs. S26–S29). Thus the observed need for metal- and oxidation/spin-state-specific LFER slopes is not a consequence of functional choice, but even the applicability of more specific LFERs will be challenged for some IS/HS states.

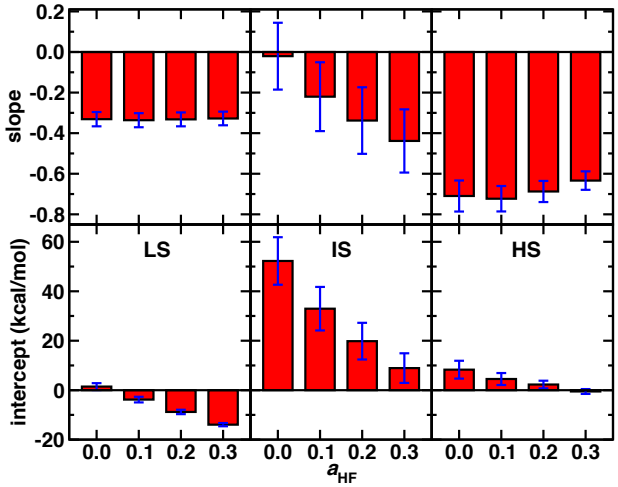

Fig. 5 Δ*E*(oxo) vs Δ*E*(HAT) LFER slopes (top) and intercepts in kcal/mol (bottom) with standard errors (shown in blue) obtained across LS (left), IS (middle), and HS (right) Fe(II) resting state catalysts as a function of HF exchange fraction, a_{HF}. Zero-axes are shown by black solid lines

Given that subtle variations in catalyst energetics cannot readily be captured by LFERs, we next evaluated the magnitude of relative catalyst performance changes by quantifying changes in percentile ranks for catalyst reaction energetics with HF exchange. These changes should highlight the extent to which catalyst energetics are shifting with respect to each other as a result of the catalyst-specific HF exchange sensitivities described in Sec 4.1. By metal, the relative oxo formation performance of Cr catalysts is least affected by a_{HF} value, whereas significant differences are observed in Δ*E*(oxo) percentile ranks for other metals (Fig. 6 and Figs. S30–S31 and Table S17). In the case of HAT, increasing a_{HF} does not frequently alter the relative favorability of either Cr or Fe catalysts, but Mn and Co catalyst performance for HAT is

strongly exchange-dependent (Fig. 6 and Figs. S30–S31 and Table S17). This suggests that the most favorable Cr catalyst for oxo formation or HAT with GGA would remain the same with moderate exchange (i.e., a_{HF} = 0.30) in a GGA hybrid, and so the poor performance of these catalysts is, as a whole, invariant to functional choice. However, this invariance does not hold true for either step for Mn or Co and only applies for HAT with Fe, which is notable since Fe is one of the most frequent targets of biomimetic catalyst design.

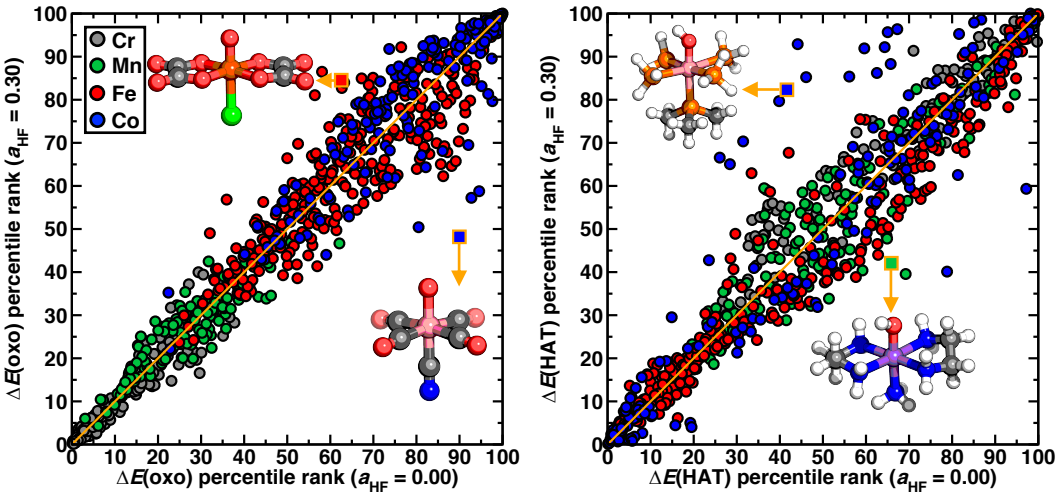

Fig. 6 Plots of percentile rank of energetics (Δ*E*(oxo), left and Δ*E*(HAT), right) at a_{HF} = 0.00 vs a_{HF} = 0.30. All catalysts are shown as data points colored by metal, with Cr in gray, Mn in green, Fe in red, and Co in blue, as shown in the inset legend in the left plot. Representative catalysts that deviate from parity are shown in outlined orange squares with arrows to inset structures: (left) Fe(V)=O(ox)$_2$(Cl$^-$) and Co(V)=O(CO)$_4$(CN$^-$) and (right) Co(IV)-OH(PH$_3$)$_4$(PMe$_3$) and Mn(IV)-OH(en)$_2$(NH$_3$), where ox = oxalate and en = ethylenediamine. Ball and stick structures are colored by element as: H in white, C in gray, N in blue, O in red, F in cyan, P in orange, Mn in purple, Fe in brown, and Co in pink. The parity line is shown in orange in both plots

In the context of method dependence in catalyst design, the relative invariance of Fe HAT percentile ranks is of considerable interest in the design of promising methane-to-methanol catalysts. Thus, we return to the question of spin-state dependence with these observations of catalyst rank, since we showed that IS LFERs were more exchange-dependent than those for LS or HS Fe(II). The IS Fe(II) catalysts indeed have the greatest exchange sensitivity in Δ*E*(oxo) percentile ranks, but they preserve the small sensitivities observed overall for Fe Δ*E*(HAT)

percentile ranks (Figs. S31–S32). The HS Fe(II) catalysts that of primary focus for catalyst design screens have even smaller exchange dependence for both ΔE(oxo) and ΔE(HAT) percentile ranks (Figs. S31–S32).

Ultimately, we should expect that trends described thus far can also be sensitive to ligand field strength. Complexes with strong field ligands are known [117,63,35,119,36] to exhibit greater exchange sensitivity than those with weak field ligands, explaining possible shifts in catalyst ranks with increasing a_{HF} values. Indeed, catalysts (e.g., with Co) with strong field (e.g., PH_3) ligands shift toward relatively favorable ΔE(oxo) and unfavorable ΔE(HAT) with increasing a_{HF} values, whereas weak field (e.g., H_2O) ligands correspond to TMCs with worsening relative ΔE(oxo) percentile rank (Fig. S33). The unexpected outliers in relative ordering for later transition metals (i.e., Fe, Co) are also typically catalysts with strong field ligands (Fig. 6 and Fig. S34). Overall, this suggests that in many cases relevant for computational catalyst design (e.g., Fe TMCs), the single most favorable catalyst for oxo formation or HAT obtained with GGA is unlikely to have the same ligand chemistry as the catalyst obtained with a hybrid functional, despite the relative insensitivity of trends obtained from global or even specific LFERs.

4.3 Trends in Spin Splitting Energies and Ground States

While we expect weak-field ligands to favor HS ground states and strong-field ligands to favor LS ground states, ground state assignment for the mid-row TMCs will also be sensitive to functional choice. Increasing HF exchange fraction from a GGA to a hybrid tends to preferentially stabilize HS states over LS states in mid-row transition metal complexes [36,117,38,120]. While spin-state splitting and ordering sensitivity is well-established over large

data sets [117], reaction energetic sensitivity has only been explored on small data sets [63,45]. Since we know that reaction energetics in our catalysts have similar HF exchange sensitivity magnitudes to those typical of ground spin state assignment, we next assess the interplay of spin-state and reaction energetics sensitivity.

A change in the reactant and product intermediate ground states for a reaction step with HF exchange alters whether the reaction is spin-allowed, i.e., the ground state is unchanged or only minimally-changed as in radical reactions. To make this assignment across a sufficiently broad catalyst set, we classify reactions as spin-allowed if the ground state is unchanged for oxo formation and HAT, which requires that the resting state and metal-oxo intermediates are in the same spin state and the metal-hydroxo intermediate differs by a single additionally unpaired electron, and we classify any energy landscape with a change in ground state as spin-forbidden. This assignment was chosen because this analysis only requires that we study the exchange-dependent spin-state ordering and splitting energies for the intermediates involved in oxo formation and HAT, allowing us a larger set than if we included the methanol-bound intermediate needed to compute release and rebound sensitivities that would have greatly reduced the available data set size (Tables S18–S19). An additional motivation for focusing on only the first two steps is that since the radical rebound step is strongly exothermic, rapid progress for this step even through a metastable spin state could be expected.

We analyze the change in distribution of ground spin states for the three intermediates (i.e., resting state, metal-oxo, and metal-hydroxo) with increasing HF exchange (Fig. 7 and Tables S20–S21 and Figs. S35–S37). The expected behavior is observed with increasing a_{HF}, with the number of catalysts with LS ground states decreasing for all three intermediates as IS and HS states become increasingly favored (Fig. 7). This is especially true for the resting state

and metal-hydroxo intermediates, which have spin splitting energies with higher exchange sensitivities than the metal-oxo intermediates do (Fig. 7 and Tables S20–S21 and Figs. S35–S37). While overall behavior of exchange to stabilize HS/IS over LS states is expected, reduced spin-state exchange sensitivity of the metal-oxo is at first surprising because the metal-oxo bond nominally contributes a stronger ligand field interaction than the resting state or metal-hydroxo intermediate. Resting state intermediates have an even stronger preference towards IS states on average in comparison to the metal-hydroxo intermediate (Fig. 7 and Figs. S38–S39).

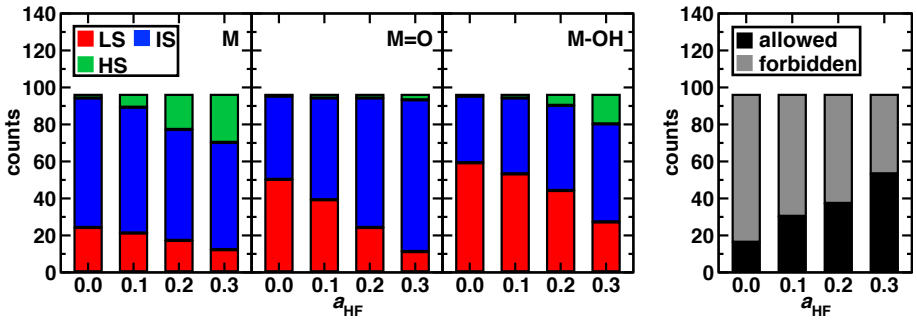

Fig. 7 Stacked bar plots of the number of catalysts that have LS (red), IS (blue), and HS (green) ground states as a function of HF exchange, a_{HF}, for resting state (M), metal-oxo (M=O), and metal-hydroxo (M-OH) intermediates. The HS state is only defined for Fe(II)/Co(III). The plot on the right shows the number of catalysts that have a spin allowed reaction energy landscape for both oxo formation and HAT steps (shown in black) and a spin forbidden landscape (shown in gray) as a function of a_{HF}

Our spin state and oxidation state convention means that HS states are only defined for a d^6 resting state (i.e., Fe(II) or Co(III)). Where sufficient data is available, as is the case for Fe(II) alone, HS states are increasingly favored instead for these same intermediates (Fig. 7 and Figs. S39). Even in the case of Fe(II), the electron-poor, metal-oxo intermediate still favors IS ground states with only a small number (i.e., 3 of 32) of Fe(II) metal-oxo intermediates becoming HS at increased exchange values (Fig. 7 and Figs. S39). When the HS state is favored for the Fe(IV)=O intermediate, it is only for the catalysts with have very weak-field ligands (e.g., H_2O, Fig. 7 and Figs. S39). Thus, a combined ligand field and delocalization argument still applies to guide understanding of HF exchange favored ground states, but a decreased difference in

delocalization of spin states in the metal-oxo due to more equivalent π interactions means this intermediate has lower spin-splitting exchange sensitivity than the resting state or metal-hydroxo intermediates. As a result of the higher spin splitting exchange sensitivities of the resting state and metal-hydroxo intermediates in Fe(II), more catalysts become spin-allowed with increasing exchange as the resting state and metal-hydroxo intermediates have increasingly stabilized IS or HS ground states that achieve consistency with an already IS or HS metal-oxo ground state (Fig. 7 and Figs. S39). For other metals and oxidation states (i.e., Cr, Mn, Co(II), and Fe(III)), the ground state of the resting state has limited exchange dependence in comparison to more moderate stabilization of the IS state for the metal-oxo and metal-hydroxo intermediates at higher a_{HF} (Fig. 7 and Fig. S38).

Given their importance in biological and biomimetic catalysis, it is notable that the Fe(II) catalysts exhibit such strong sensitivity of spin-state ordering by intermediate to HF exchange. While the resting state and metal-hydroxo intermediates show increasingly stable HS ground states at higher HF exchange fractions, the metal-oxo intermediate typically (> 90%) has an IS ground state irrespective of HF exchange fraction and thus spin-forbidden reaction energetics (Tables S22–S23). Examining representative Fe(II) catalysts, we note that the Fe(II)$(H_2O)_4$(pisc) catalyst with weak-field ligands has spin-forbidden energetics at a_{HF} = 0.0 with distinct ground states for all three intermediates (i.e., HS resting state, IS metal-oxo, and LS metal-hydroxo, Fig. 8). Higher exchange fractions ($a_{HF} \geq 0.1$) stabilize HS ground states for both metal-oxo and metal-hydroxo, leading to a spin-allowed reaction in a HS ground state that is consistent with ligand field arguments (Fig. 8). In contrast, an Fe(II)$(PF_3)_4(H_2O)$ catalyst with strong field ligands has spin-forbidden energetics regardless of a_{HF} values (Fig. 8). For this catalyst, the GGA (i.e., a_{HF} = 0.0) oxo formation is spin-allowed in an IS state that is consistent with ligand field

arguments, but it becomes spin-forbidden at higher a_{HF} values that stabilize an HS state for the resting state intermediate while the metal-oxo IS ground state remains unchanged (Fig. 8). Hence, the functional choice impacts conclusions on spin-allowed or spin-forbidden reactivity due to differences in spin-state ordering sensitivity by intermediate, an effect that is particularly evident for Fe(II) catalysts due to the near degeneracy of the three spin states studied.

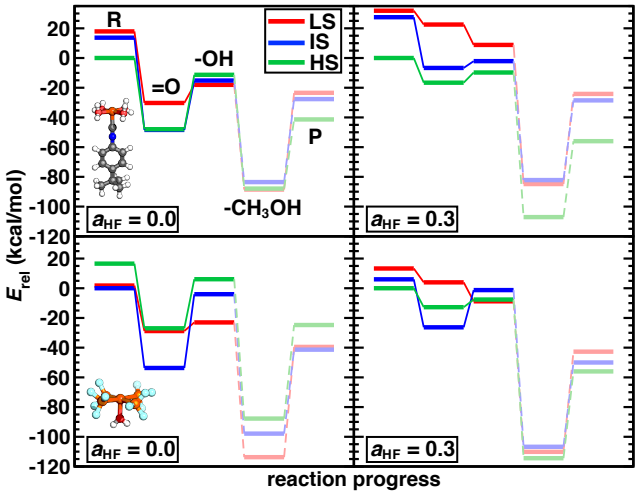

Fig. 8 HF exchange effect on ground spin states demonstrated with two representative Fe(II) catalysts, Fe(II)$(H_2O)_4$(pisc) (top) and Fe(II)$(PF_3)_4(H_2O)$ (bottom). Reaction thermodynamics are shown for LS (red), IS (blue), and HS (green) states at a_{HF} = 0.0 (left) and a_{HF} = 0.3 (right). Reactant, metal-oxo, metal-hydroxo, methanol-bound intermediate, and product are denoted by R, =O, -OH, -CH_3OH, and P, respectively. Reaction thermodynamics of oxo formation and HAT steps are shown in opaque colors while those of rebound and methanol release steps are indicated with dashed lines and translucent colors

5 Conclusions

Typically, high-throughput catalyst screens are carried out with a single DFT functional at a fixed degree of HF exchange, either none as is common in plane wave periodic boundary condition calculations for heterogeneous catalysis or around a_{HF} = 0.20-0.25 in molecular catalysis. We carried out the first large-scale study of the effects of HF exchange on over 1,200 mononuclear 3*d* TMCs in a range of oxidation and spin states to understand the effects of these choices on computed reaction energetics in the representative case of direct methane-to-methanol

conversion via a radical rebound mechanism. With increasing exchange, we observed less favorable ΔE(oxo) but more favorable ΔE(HAT) and ΔE(rebound), while ΔE(release) had limited functional sensitivity. The average sensitivities of the first three steps were comparable to typical sensitivities observed for spin splitting energetics [46] and those reported previously on model catalysts [63]. As a result of these sensitivities, the mostly exothermic ΔE(oxo) becomes more endothermic with increasing exchange, whereas the mostly endothermic ΔE(HAT) becomes increasingly exothermic at higher a_{HF}. We observed wide ranges of sensitivities that depended on catalyst chemistry, leading to cases where different exchange fractions would predict distinct "best-in-class" catalysts for each reaction step, as quantified through changes in percentile rank with exchange.

We showed that differences in the applicability and slopes for global oxo formation vs HAT scaling relationships obtained with a GGA [77,81] vs a hybrid [88] were due to differences in data set construction and not functional choice. Indeed, we observed global LFERs to be insensitive to HF exchange fraction but also to have too high fitting errors to be useful at any a_{HF} value. Analysis of oxidation- and spin-state dependent LFERs by metal indicated that LS LFER slopes were insensitive to HF exchange, whereas for Fe(II) where both IS and HS LFER slopes could be obtained, IS states were disproportionately sensitive. Thus, applicability of a global LFER to open shell metal centers that has sometimes been observed [81] is likely specific to the range of spin states for the systems studied.

We showed the interplay of the effect of exchange on spin-splitting energetics and reaction energetics to be important to computational screening of open-shell catalysts where the possibility of multi-state reactivity[98,100] necessitates analysis of whether the reaction is spin-allowed or spin-forbidden. As might be expected from the typical effect of HF exchange to

stabilize higher-spin states, we observed a decrease in the number of LS ground states vs IS or HS ground states, but the effect was stronger in resting state or metal-hydroxo intermediates than already IS-favoring metal-oxos. Given that increasing exchange had the effect of aligning the metal-oxo ground state with the other two intermediates, increasing HF exchange generally recovered a greater number of catalysts with spin-allowed energetics and predicted more consistent, expected ground states for catalysts with weak ligand fields.

Overall, by studying the representative case of direct methane-to-methanol conversion we have shown that the functional choice can alter relative energetics, catalyst performance, and whether the reaction is spin-allowed. For LS states of all metals studied, however, the relative trade-off between oxo formation and HAT energetics is not strongly functional sensitive, as evident from the limited HF exchange dependence of LS-specific LFERs. Thus, LFERs for catalytic cycles with closed shell intermediates remain a useful way to draw conclusions from a single approximate DFT functional.

DECLARATIONS

Funding: This research was funded in the form of support to V.V. and A.N. by the National Science Foundation (grant numbers CBET-1704266 and CBET-1846426), a National Science Foundation Graduate Research Fellowship under Grant #1122374 (to A.N.). Partial support for conception and data set generation for this study was supported by the Department of Energy under grant number DE-SC0012702. Algorithm and workflow development as well as data collection strategies were supported by the Office of Naval Research under grant numbers N00014-17-1-2956, N00014-18-1-2434, and N00014-20-1-2150. H.J.K. holds a Career Award at the Scientific Interface from the Burroughs Wellcome Fund, an AAAS Marion Milligan Mason Award, and an Alfred P. Sloan Fellowship in Chemistry, which supported this work. This work was carried out in part using computational resources from the Extreme Science and Engineering Discovery Environment (XSEDE), which is supported by National Science Foundation grant number ACI-1548562.

Conflicts of interest: The authors declare that they have no conflict of interest.

Availability of data and material: Electronic supplementary material available.

Description of Electronic Supplementary material. Geometry criteria to evaluate fidelity of optimized geometries; number of systems retained and eliminated after filtering process; summary of checks done after computing linearized exchange sensitivities; number of catalysts common to oxo formation and HAT steps after filtering process; statistics of catalysts common to oxo formation and HAT steps by M(OS) for which ground state can be determined; number of catalysts common to all four reaction steps after filtering process; histogram of standard deviation of ΔE(release) computed at different a_{HF}; statistics of catalysts common to all four reaction steps by M(OS) for which ground state can be determined; Co catalysts with negative ΔE(oxo) sensitivities; optimized geometries of Co catalysts with negative ΔE(oxo) sensitivities; list of Cr, Mn, and Fe catalysts with positive ΔE(rebound) sensitivities; optimized geometries of catalysts with positive ΔE(rebound) sensitivities; average sensitivities for ΔE(oxo), ΔE(HAT), and ΔE(rebound) by metal; normalized histograms of sensitivities of all four reaction steps by metal; optimized geometries of representative catalysts comparing sensitivities; average sensitivities of ΔE(oxo), ΔE(HAT), and ΔE(rebound) by OS; stacked histograms of sensitivities for all four reaction steps by metal oxidation (M(OS))/spin; average sensitivities of ΔE(oxo), ΔE(HAT), and ΔE(rebound) by M(OS)/spin; plot of sensitivities of oxo formation and HAT reaction steps; stacked histograms of ΔE(oxo) and ΔE(HAT) obtained at a_{HF} = 0.00, 0.10, 0.20, and 0.30; number of catalysts in four quadrants on ΔE(oxo) vs ΔE(HAT) plot; number of catalysts in four quadrants on ΔE(oxo) vs ΔE(HAT) plot by metal; stacked bar plot of number of catalysts in four quadrants; stacked bar plot of number of catalysts in four quadrants by metal; optimized geometries of Mn catalysts with exothermic ΔE(HAT); statistics of ΔE(oxo) and ΔE(HAT) by metal at a_{HF} = 0.00, 0.10, 0.20, and 0.30; range of ΔE(oxo) and ΔE(HAT) by metal at a_{HF} = 0.00 and 0.30; ΔE(oxo) vs ΔE(HAT) of Cr(II), Cr(III), Mn(II), Mn(III), Fe(II), Fe(III), Co(II), and Co(III) catalysts obtained at a_{HF} = 0.00, 0.10, 0.20, and 0.30; LFER regressions over ΔE(oxo) vs ΔE(HAT) data; ΔE(oxo) vs ΔE(HAT) global LFERs of all catalysts; ΔE(oxo) vs ΔE(HAT) LFERs of Cr(II), Cr(III), Mn(II), Mn(III), Fe(III), Co(II), and Co(III) catalysts; average vs standard deviation of percentile rank of ΔE(oxo) and ΔE(HAT); average of percentile rank of ΔE(oxo) vs ΔE(HAT) of all catalysts; SRCC of percentile ranks of ΔE(oxo) and ΔE(HAT) by M(OS)/spin; average of percentile rank of ΔE(oxo) vs ΔE(HAT) of Fe and Co catalysts; representative catalysts showing comparison of percentile ranks; HS-LS spin splitting energy sensitivities for Fe(II) catalysts; classification of all reaction energies as spin-allowed or spin-forbidden; average and standard deviation of IS-LS spin splitting energy sensitivities for all catalysts; average and standard deviation of all three spin splitting energy sensitivities for Fe(II) catalysts; histograms of IS-LS, HS-IS, and HS-LS spin splitting energy sensitivities; stacked bar plots of ground spin states of all catalyst intermediates; stacked bar plots of ground spin states of Fe(II) catalyst intermediates; ground spin states of intermediates of Fe(II) catalysts at a_{HF} = 0.00 and 0.30; classification of Fe(II) reaction energies as spin-allowed or spin-forbidden. (PDF)

The data sets and codes generated during and/or analyzed during the current study are available in the "methane-to-methanol reaction energy sensitivities" repository, at https://doi.org/10.5281/zenodo.4895418 The codes used in this work are also added to molSimplify.

Author contributions: All authors contributed to the study conception and design. Data collection and analysis were performed by Vyshnavi Vennelakanti and Aditya Nandy. The first draft of the manuscript was written by Vyshnavi Vennelakanti, revised by Heather J. Kulik, and all authors commented on and revised versions of the manuscript. All authors read and approved the final manuscript.

References

1. Spivey JJ, Krishna KS, Kumar CSSR, Dooley KM, Flake JC, Haber LH, Xu Y, Janik MJ, Sinnott SB, Cheng YT, Liang T, Sholl DS, Manz TA, Diebold U, Parkinson GS, Bruce DA, de Jongh P (2014) Synthesis, Characterization, and Computation of Catalysts at the Center for Atomic-Level Catalyst Design. J Phys Chem C 118 (35):20043-20069
2. Sperger T, Sanhueza IA, Kalvet I, Schoenebeck F (2015) Computational Studies of Synthetically Relevant Homogeneous Organometallic Catalysis Involving Ni, Pd, Ir, and Rh: An Overview of Commonly Employed DFT Methods and Mechanistic Insights. Chem Rev 115 (17):9532-9586
3. Sperger T, Sanhueza IA, Schoenebeck F (2016) Computation and Experiment: A Powerful Combination to Understand and Predict Reactivities. Accounts Chem Res 49 (6):1311-1319
4. Medford AJ, Vojvodic A, Hummelshoj JS, Voss J, Abild-Pedersen F, Studt F, Bligaard T, Nilsson A, Norskov JK (2015) From the Sabatier Principle to a Predictive Theory of Transition-Metal Heterogeneous Catalysis. J Catal 328:36-42
5. Cheng GJ, Zhang XH, Chung LW, Xu LP, Wu YD (2015) Computational Organic Chemistry: Bridging Theory and Experiment in Establishing the Mechanisms of Chemical Reactions. Journal of the American Chemical Society 137 (5):1706-1725
6. Vogiatzis KD, Polynski MV, Kirkland JK, Townsend J, Hashemi A, Liu C, Pidko EA (2018) Computational approach to molecular catalysis by 3d transition metals: Challenges and opportunities. Chem Rev 119 (4):2453-2523
7. Raugei S, DuBois DL, Rousseau R, Chen S, Ho M-H, Bullock RM, Dupuis M (2015) Toward Molecular Catalysts by Computer. Accounts Chem Res 48 (2):248-255
8. Greeley J (2016) Theoretical heterogeneous catalysis: scaling relationships and computational catalyst design. Annual review of chemical and biomolecular engineering 7:605-635
9. Nørskov JK, Bligaard T, Rossmeisl J, Christensen CH (2009) Towards the computational design of solid catalysts. Nature chemistry 1 (1):37-46
10. Foscato M, Jensen VR (2020) Automated in silico design of homogeneous catalysts. ACS Catalysis 10 (3):2354-2377
11. Nandy A, Zhu J, Janet JP, Duan C, Getman RB, Kulik HJ (2019) Machine Learning Accelerates the Discovery of Design Rules and Exceptions in Stable Metal-Oxo Intermediate Formation. ACS Catalysis 9:8243-8255
12. Vogiatzis KD, Haldoupis E, Xiao DJ, Long JR, Siepmann JI, Gagliardi L (2016) Accelerated Computational Analysis of Metal–Organic Frameworks for Oxidation Catalysis. The Journal of Physical Chemistry C 120 (33):18707-18712. doi:10.1021/acs.jpcc.6b07115
13. Kim JY, Kulik HJ (2018) When is Ligand pKa a Good Descriptor for Catalyst Energetics? In Search of Optimal CO_2 Hydration Catalysts. J Phys Chem A 122:4579-4590
14. Gani TZH, Kulik HJ (2018) Understanding and Breaking Scaling Relations in Single-Site Catalysis: Methane to Methanol Conversion by Fe^{IV}=O. ACS Catalysis 8:975-986

15. Cramer CJ, Truhlar DG (2009) Density functional theory for transition metals and transition metal chemistry. Physical Chemistry Chemical Physics 11 (46):10757-10816
16. Janet JP, Zhao Q, Ioannidis EI, Kulik HJ (2017) Density functional theory for modelling large molecular adsorbate-surface interactions: a mini-review and worked example. Mol Simulat 43 (5-6):327-345
17. Gaggioli CA, Stoneburner SJ, Cramer CJ, Gagliardi L (2019) Beyond Density Functional Theory: The Multiconfigurational Approach To Model Heterogeneous Catalysis. ACS Catal 9 (9):8481-8502
18. Jimenez-Hoyos CA, Janesko BG, Scuseria GE (2009) Evaluation of Range-Separated Hybrid and Other Density Functional Approaches on Test Sets Relevant for Transition Metal-Based Homogeneous Catalysts. J Phys Chem A 113 (43):11742-11749
19. Zhao Q, Kulik HJ (2019) Stable Surfaces That Bind Too Tightly: Can Range-Separated Hybrids or DFT+ U Improve Paradoxical Descriptions of Surface Chemistry? The journal of physical chemistry letters 10 (17):5090-5098
20. Schimka L, Harl J, Stroppa A, Grüneis A, Marsman M, Mittendorfer F, Kresse G (2010) Accurate surface and adsorption energies from many-body perturbation theory. Nature materials 9 (9):741-744
21. Kulik HJ (2015) Perspective: Treating electron over-delocalization with the DFT plus U method. J Chem Phys 142 (24)
22. Yu HS, Li SL, Truhlar DG (2016) Perspective: Kohn-Sham density functional theory descending a staircase. The Journal of chemical physics 145 (13):130901
23. Cohen AJ, Mori-Sanchez P, Yang W (2008) Fractional Charge Perspective on the Band Gap in Density-Functional Theory. Physical Review B 77 (11)
24. Perdew JP, Parr RG, Levy M, Balduz JL, Jr. (1982) Density-Functional Theory for Fractional Particle Number - Derivative Discontinuities of the Energy. Phys Rev Lett 49 (23):1691-1694
25. Yang WT, Zhang YK, Ayers PW (2000) Degenerate ground states and a fractional number of electrons in density and reduced density matrix functional theory. Phys Rev Lett 84 (22):5172-5175
26. Cohen AJ, Mori-Sanchez P, Yang W (2008) Insights into Current Limitations of Density Functional Theory. Science 321 (5890):792-794
27. Janesko BG, Proynov E, Kong J, Scalmani G, Frisch MJ (2017) Practical density functionals beyond the overdelocalization–underbinding zero-sum game. The journal of physical chemistry letters 8 (17):4314-4318
28. Johnson BG, Gonzales CA, Gill PMW, Pople JA (1994) A Density-Functional Study of the Simplest Hydrogen Abstraction Reaction - Effect of Self-Interaction Correction. Chem Phys Lett 221 (1-2):100-108
29. Ruzsinszky A, Perdew JP, Csonka GI, Vydrov OA, Scuseria GE (2006) Spurious fractional charge on dissociated atoms: Pervasive and resilient self-interaction error of common density functionals. J Chem Phys 125 (19)
30. Ruzsinszky A, Perdew JP, Csonka GI, Vydrov OA, Scuseria GE (2007) Density functionals that are one- and two- are not always many-electron self-interaction-free, as shown for H-2(+), He-2(+), LiH+, and Ne-2(+). J Chem Phys 126 (10)
31. Dutoi AD, Head-Gordon M (2006) Self-Interaction Error of Local Density Functionals for Alkali-Halide Dissociation. Chem Phys Lett 422 (1-3):230-233
32. Bally T, Sastry GN (1997) Incorrect Dissociation Behavior of Radical Ions in Density Functional Calculations. J Phys Chem A 101 (43):7923-7925

33. Zhang Y, Yang W (1998) A Challenge for Density Functionals: Self-Interaction Error Increases for Systems with a Noninteger Number of Electrons. J Chem Phys 109 (7):2604-2608
34. Wilbraham L, Verma P, Truhlar DG, Gagliardi L, Ciofini I (2017) Multiconfiguration Pair-Density Functional Theory Predicts Spin State Ordering in Iron Complexes with the Same Accuracy as Complete Active Space Second-Order Perturbation Theory at a Significantly Reduced Computational Cost. J Phys Chem Lett 8 (9):2026-2030
35. Ioannidis EI, Kulik HJ (2017) Ligand-Field-Dependent Behavior of Meta-GGA Exchange in Transition-Metal Complex Spin-State Ordering. J Phys Chem A 121 (4):874-884
36. Ioannidis EI, Kulik HJ (2015) Towards quantifying the role of exact exchange in predictions of transition metal complex properties. J Chem Phys 143 (3)
37. Mortensen SR, Kepp KP (2015) Spin Propensities of Octahedral Complexes From Density Functional Theory. J Phys Chem A 119 (17):4041-4050
38. Droghetti A, Alfe D, Sanvito S (2012) Assessment of density functional theory for iron(II) molecules across the spin-crossover transition. J Chem Phys 137 (12)
39. Ganzenmuller G, Berkaine N, Fouqueau A, Casida ME, Reiher M (2005) Comparison of Density Functionals for Differences between the High-(T-5(2g)) and Low-((1)A(1g)) Spin States of Iron(II) Compounds. IV. Results for the Ferrous Complexes [Fe(L)('NHS4')]. J Chem Phys 122 (23)
40. Kulik HJ, Cococcioni M, Scherlis DA, Marzari N (2006) Density functional theory in transition-metal chemistry: A self-consistent Hubbard U approach. Phys Rev Lett 97 (10)
41. Tozer DJ, De Proft F (2005) Computation of the hardness and the problem of negative electron affinities in density functional theory. J Phys Chem A 109 (39):8923-8929
42. Teale AM, De Proft F, Tozer DJ (2008) Orbital energies and negative electron affinities from density functional theory: Insight from the integer discontinuity. J Chem Phys 129 (4)
43. Peach MJG, Teale AM, Helgaker T, Tozer DJ (2015) Fractional Electron Loss in Approximate DFT and Hartree-Fock Theory. J Chem Theory Comput 11 (11):5262-5268
44. Mori-Sanchez P, Cohen AJ, Yang WT (2008) Localization and delocalization errors in density functional theory and implications for band-gap prediction. Phys Rev Lett 100 (14)
45. Mahler A, Janesko BG, Moncho S, Brothers EN (2018) When Hartree-Fock exchange admixture lowers DFT-predicted barrier heights: Natural bond orbital analyses and implications for catalysis. J Chem Phys 148 (24)
46. Janet JP, Kulik HJ (2017) Predicting Electronic Structure Properties of Transition Metal Complexes with Neural Networks. Chemical Science 8:5137-5152. doi:10.1039/C7SC01247K
47. Reiher M, Salomon O, Hess BA (2001) Reparameterization of hybrid functionals based on energy differences of states of different multiplicity. Theoretical Chemistry Accounts 107 (1):48-55
48. Coskun D, Jerome SV, Friesner RA (2016) Evaluation of the performance of the B3LYP, PBE0, and M06 DFT functionals, and DBLOC-corrected versions, in the calculation of redox potentials and spin splittings for transition metal containing systems. Journal of chemical theory and computation 12 (3):1121-1128
49. Haunschild R, Henderson TM, Jimenez-Hoyos CA, Scuseria GE (2010) Many-electron self-interaction and spin polarization errors in local hybrid density functionals. J Chem Phys 133 (13)
50. Mori-Sanchez P, Cohen AJ, Yang WT (2006) Many-electron self-interaction error in approximate density functionals. J Chem Phys 125 (20)
51. Schmidt T, Kummel S (2016) One- and many-electron self-interaction error in local and global hybrid functionals. Phys Rev B 93 (16)

52. Kim MC, Sim E, Burke K (2013) Understanding and Reducing Errors in Density Functional Calculations. Phys Rev Lett 111 (7)
53. Zheng X, Liu M, Johnson ER, Contreras-Garcia J, Yang W (2012) Delocalization Error of Density-Functional Approximations: A Distinct Manifestation in Hydrogen Molecular Chains. J Chem Phys 137 (21): 214106
54. Simm GN, Reiher M (2016) Systematic error estimation for chemical reaction energies. Journal of chemical theory and computation 12 (6):2762-2773
55. Sutton JE, Guo W, Katsoulakis MA, Vlachos DG (2016) Effects of correlated parameters and uncertainty in electronic-structure-based chemical kinetic modelling. Nature chemistry 8 (4):331-337
56. Walker E, Ammal SC, Terejanu GA, Heyden A (2016) Uncertainty quantification framework applied to the water–gas shift reaction over Pt-based catalysts. The Journal of Physical Chemistry C 120 (19):10328-10339
57. Wellendorff J, Lundgaard KT, Mogelhoj A, Petzold V, Landis DD, Norskov JK, Bligaard T, Jacobsen KW (2012) Density functionals for surface science: Exchange-correlation model development with Bayesian error estimation. Phys Rev B 85 (23)
58. Medford AJ, Wellendorff J, Vojvodic A, Studt F, Abild-Pedersen F, Jacobsen KW, Bligaard T, Norskov JK (2014) Assessing the reliability of calculated catalytic ammonia synthesis rates. Science 345 (6193):197-200
59. Sumaria V, Krishnamurthy D, Viswanathan V (2018) Quantifying Confidence in DFT Predicted Surface Pourbaix Diagrams and Associated Reaction Pathways for Chlorine Evolution. ACS Catal 8 (10):9034-9042
60. Christensen R, Hansen HA, Vegge T (2015) Identifying systematic DFT errors in catalytic reactions. Catal Sci Technol 5 (11):4946-4949
61. Wellendorff J, Silbaugh TL, Garcia-Pintos D, Norskov JK, Bligaard T, Studt F, Campbell CT (2015) A benchmark database for adsorption bond energies to transition metal surfaces and comparison to selected DFT functionals. Surf Sci 640:36-44
62. Houchins G, Viswanathan V (2017) Quantifying confidence in density functional theory predictions of magnetic ground states. Phys Rev B 96 (13)
63. Gani TZH, Kulik HJ (2017) Unifying Exchange Sensitivity in Transition Metal Spin-State Ordering and Catalysis Through Bond Valence Metrics Journal of Chemical Theory and Computation 13:5443-5457
64. Busch M, Fabrizio A, Luber S, Hutter J, Corminboeuf C (2018) Exploring the Limitation of Molecular Water Oxidation Catalysts. The Journal of Physical Chemistry C 122 (23):12404-12412. doi:10.1021/acs.jpcc.8b03935
65. Janesko BG, Scuseria GE (2008) Hartree-Fock orbitals significantly improve the reaction barrier heights predicted by semilocal density functionals. J Chem Phys 128 (24)
66. Gani TZH, Kulik HJ (2016) Where Does the Density Localize? Convergent Behavior for Global Hybrids, Range Separation, and DFT+U Journal of Chemical Theory and Computation 12:5931-5945
67. Liu F, Kulik HJ (2020) Impact of Approximate DFT Density Delocalization Error on Potential Energy Surfaces in Transition Metal Chemistry. Journal of Chemical Theory and Computation 16 (1):264-277
68. Oloo W, N., Que L, Jr. (2015) Bioinspired Nonheme Iron Catalysts for C-H and C-C Bond Oxidation: Insights into the Nature of the Metal-Based Oxidants. Accounts Chem Res 48 (9):2612-2621. doi:10.1021/acs.accounts.5b00053

69. Que L, Jr., Tolman WB (2008) Biologically Inspired Oxidation Catalysis. Nature 455 (7211):333-340. doi:10.1038/nature07371
70. Biswas AN, Puri M, Meier KK, Oloo WN, Rohde GT, Bominaar EL, Munck E, Que L, Jr. (2015) Modeling TauD-J: a High-Spin Nonheme Oxoiron(IV) Complex with High Reactivity Toward C-H Bonds. Journal of the American Chemical Society 137 (7):2428-2431. doi:10.1021/ja511757j
71. Engelmann X, Monte-Perez I, Ray K (2016) Oxidation Reactions with Bioinspired Mononuclear Non-Heme Metal-Oxo Complexes. Angewandte Chemie International Edition 55 (27):7632-7649. doi:10.1002/anie.201600507
72. Hammond C, Forde MM, Rahim A, Hasbi M, Thetford A, He Q, Jenkins RL, Dimitratos N, Lopez‐Sanchez JA, Dummer NF (2012) Direct Catalytic Conversion of Methane to Methanol in an Aqueous Medium by Using Copper‐Promoted Fe‐ZSM‐5. Angew Chem, Int Ed 51 (21):5129-5133
73. Jones C, Taube D, Ziatdinov VR, Periana RA, Nielsen RJ, Oxgaard J, Goddard WA (2004) Selective Oxidation of Methane to Methanol Catalyzed, with C-H Activation, by Homogeneous, Cationic Gold. Angew Chem, Int Ed 116 (35):4726-4729
74. Palkovits R, Antonietti M, Kuhn P, Thomas A, Schüth F (2009) Solid Catalysts for the Selective Low‐Temperature Oxidation of Methane to Methanol. Angewandte Chemie International Edition 48 (37):6909-6912
75. Hull JF, Balcells D, Sauer EL, Raynaud C, Brudvig GW, Crabtree RH, Eisenstein O (2010) Manganese Catalysts for C-H Activation: An Experimental/Theoretical Study Identifies the Stereoelectronic Factor that Controls the Switch between Hydroxylation and Desaturation Pathways. Journal of the American Chemical Society 132 (22):7605-7616. doi:10.1021/ja908744w
76. Balcells D, Moles P, Blakemore JD, Raynaud C, Brudvig GW, Crabtree RH, Eisenstein O (2009) Molecular Recognition in Mn-Catalyzed C-H Oxidation. Reaction Mechanism and Origin of Selectivity from a DFT Perspective. Dalton Transactions (30):5989-6000
77. Latimer AA, Kulkarni AR, Aljama H, Montoya JH, Yoo JS, Tsai C, Abild-Pedersen F, Studt F, Nørskov JK (2017) Understanding Trends in C-H Bond Activation in Heterogeneous Catalysis. Nature Materials 16 (2):225-229. doi:10.1038/nmat4760
78. Christensen R, Hansen HA, Dickens CF, Nørskov JK, Vegge T (2016) Functional Independent Scaling Relation for ORR/OER Catalysts. The Journal of Physical Chemistry C 120 (43):24910-24916. doi:10.1021/acs.jpcc.6b09141
79. Fajin JLC, Vines F, Cordeiro MNDS, Illas F, Gomes JRB (2016) Effect of the Exchange-Correlation Potential on the Transferability of Bronsted-Evans-Polanyi Relationships in Heterogeneous Catalysis. Journal of Chemical Theory and Computation 12 (5):2121-2126
80. Curnan MT, Kitchin JR (2015) Investigating the energetic ordering of stable and metastable TiO2 polymorphs using DFT+ U and hybrid functionals. The Journal of Physical Chemistry C 119 (36):21060-21071
81. Rosen AS, Notestein JM, Snurr RQ (2019) Structure–Activity Relationships That Identify Metal–Organic Framework Catalysts for Methane Activation. ACS Catalysis 9 (4):3576-3587. doi:10.1021/acscatal.8b05178
82. Liao P, Getman RB, Snurr RQ (2017) Optimizing Open Iron Sites in Metal−Organic Frameworks for Ethane Oxidation: A First-Principles Study. ACS Appl Mater Interfaces 9:33484-33492. doi:10.1021/acsami.7b02195

83. Pellizzeri S, Jones IA, Doan HA, Snurr RQ, Getman RB (2016) Using Gas-Phase Clusters to Screen Porphyrin-Supported Nanocluster Catalysts for Ethane Oxidation to Ethanol. Catalysis Letters 146 (12):2566-2573. doi:10.1007/s10562-016-1890-7
84. Wodrich MD, Sawatlon B, Busch M, Corminboeuf C (2021) The Genesis of Molecular Volcano Plots. Accounts Chem Res 54 (5):1107-1117
85. Anand M, Rohr B, Statt MJ, Nørskov JK (2020) Scaling Relationships and Volcano Plots in Homogeneous Catalysis. The Journal of Physical Chemistry Letters 11 (20):8518-8526
86. Busch M, Wodrich MD, Corminboeuf C (2015) Linear scaling relationships and volcano plots in homogeneous catalysis–revisiting the Suzuki reaction. Chemical science 6 (12):6754-6761
87. Andrikopoulos PC, Michel C, Chouzier S, Sautet P (2015) In Silico screening of Iron-Oxo catalysts for CH bond cleavage. ACS Catalysis 5 (4):2490-2499
88. Nandy A, Kulik HJ (2020) Why Conventional Design Rules for C–H Activation Fail for Open-Shell Transition-Metal Catalysts. ACS Catalysis 10 (24):15033-15047. doi:10.1021/acscatal.0c04300
89. Szécsényi Á, Khramenkova E, Chernyshov IY, Li G, Gascon J, Pidko EA (2019) Breaking Linear Scaling Relationships with Secondary Interactions in Confined Space: A Case Study of Methane Oxidation by Fe/ZSM-5 Zeolite. ACS Catalysis 9 (10):9276-9284. doi:10.1021/acscatal.9b01914
90. Pérez-Ramírez J, López N (2019) Strategies to break linear scaling relationships. Nature Catalysis 2 (11):971-976
91. Abram S-L, Monte-Perez I, Pfaff FF, Farquhar ER, Ray K (2014) Evidence of Two-State Reactivity in Alkane Hydroxylation by Lewis-Acid Bound Copper-Nitrene Complexes. Chemical Communications 50 (69):9852-9854
92. Zhu B, Guan W, Yan L-K, Su Z-M (2016) Two-State Reactivity Mechanism of Benzene C-C Activation by Trinuclear Titanium Hydride. Journal of the American Chemical Society 138 (35):11069-11072
93. Schwarz H (2017) Menage-a-trois: single-atom catalysis, mass spectrometry, and computational chemistry. Catal Sci Technol 7 (19):4302-4314
94. Liu WG, Zhang LL, Liu X, Liu XY, Yang XF, Miao S, Wang WT, Wang AQ, Zhang T (2017) Discriminating Catalytically Active FeNx Species of Atomically Dispersed Fe-N-C Catalyst for Selective Oxidation of the C-H Bond. Journal of the American Chemical Society 139 (31):10790-10798
95. Ricciarelli D, Belpassi L, Harvey JN, Belanzoni P (2020) Spin-Forbidden Reactivity of Transition Metal Oxo Species: Exploring the Potential Energy Surfaces. Chem Eur J 26 (14):3080-3089. doi:10.1002/chem.201904314
96. Harvey JN (2007) Understanding the Kinetics of Spin-Forbidden Chemical Reactions. Phys Chem Chem Phys 9 (3):331-343. doi:10.1039/b614390c
97. Harvey JN (2014) Spin-Forbidden Reactions: Computational Insight into Mechanisms and Kinetics. Wiley Interdisciplinary Reviews: Computational Molecular Science 4 (1):1-14. doi:10.1002/wcms.1154
98. Hirao H, Kumar D, Que L, Jr., Shaik S (2006) Two-State Reactivity in Alkane Hydroxylation by Non-Heme Iron-Oxo Complexes. Journal of the American Chemical Society 128 (26):8590-8606. doi:10.1021/ja061609o
99. Shaik S, Danovich D, Fiedler A, Schroder D, Schwarz H (1995) 2-State Reactivity in Organometallic Gas-Phase Ion Chemistry. Helv Chim Acta 78 (6):1393-1407

100. Schroder D, Shaik S, Schwarz H (2000) Two-state reactivity as a new concept in organometallic chemistry. Accounts Chem Res 33 (3):139-145
101. Groves JT, McClusky GA (1976) Aliphatic Hydroxylation via Oxygen Rebound. Oxygen Transfer Catalyzed by Iron. Journal of the American Chemical Society 98 (3):859-861. doi:10.1021/ja00419a049
102. Ufimtsev IS, Martinez TJ (2009) Quantum Chemistry on Graphical Processing Units. 3. Analytical Energy Gradients, Geometry Optimization, and First Principles Molecular Dynamics. Journal of Chemical Theory and Computation 5 (10):2619-2628
103. Ioannidis EI, Gani TZH, Kulik HJ (2016) molSimplify: A Toolkit for Automating Discovery in Inorganic Chemistry. Journal of Computational Chemistry 37:2106-2117. doi:10.1002/jcc.24437
104. O'Boyle NM, Banck M, James CA, Morley C, Vandermeersch T, Hutchison GR (2011) Open Babel: An Open Chemical Toolbox. Journal of Cheminformatics 3:33. doi:10.1186/1758-2946-3-33
105. O'Boyle NM, Morley C, Hutchison GR (2008) Pybel: a Python Wrapper for the OpenBabel Cheminformatics Toolkit. Chemistry Central Journal 2:5. doi:10.1186/1752-153X-2-5
106. Nandy A, Duan C, Janet JP, Gugler S, Kulik HJ (2018) Strategies and Software for Machine Learning Accelerated Discovery in Transition Metal Chemistry. Industrial & Engineering Chemistry Research 57 (42):13973-13986
107. Lee C, Yang W, Parr RG (1988) Development of the Colle-Salvetti Correlation-Energy Formula into a Functional of the Electron Density. Physical Review B 37:785-789
108. Becke AD (1993) Density-Functional Thermochemistry. III. The Role of Exact Exchange. The Journal of Chemical Physics 98 (7):5648-5652
109. Stephens PJ, Devlin FJ, Chabalowski CF, Frisch MJ (1994) Ab Initio Calculation of Vibrational Absorption and Circular Dichroism Spectra Using Density Functional Force Fields. The Journal of Physical Chemistry 98 (45):11623-11627
110. Grimme S, Antony J, Ehrlich S, Krieg H (2010) A Consistent and Accurate Ab Initio Parametrization of Density Functional Dispersion Correction (DFT-D) for the 94 Elements H-Pu. The Journal of Chemical Physics 132 (15):154104
111. Becke AD, Johnson ER (2005) A Density-Functional Model of the Dispersion Interaction. The Journal of Chemical Physics 123 (15):154101
112. Wadt WR, Hay PJ (1985) Ab Initio Effective Core Potentials for Molecular Calculations. Potentials for Main Group Elements Na to Bi. The Journal of Chemical Physics 82 (1):284-298. doi:10.1063/1.448800
113. Hay PJ, Wadt WR (1985) Ab Initio Effective Core Potentials for Molecular Calculations. Potentials for the Transition Metal Atoms Sc to Hg. The Journal of Chemical Physics 82 (1):270-283
114. Ditchfield R, Hehre WJ, Pople JA (1971) Self-Consistent Molecular-Orbital Methods .9. Extended Gaussian-Type Basis for Molecular-Orbital Studies of Organic Molecules. J Chem Phys 54 (2):724-+
115. Wang L-P, Song C (2016) Geometry Optimization Made Simple with Translation and Rotation Coordinates. The Journal of Chemical Physics 144 (21):214108
116. Saunders VR, Hillier IH (1973) A "Level-Shifting" Method for Converging Closed Shell Hartree-Fock Wave Functions. International Journal of Quantum Chemistry 7 (4):699-705. doi:10.1002/qua.560070407

117. Nandy A, Chu DBK, Harper DR, Duan C, Arunachalam N, Cytter Y, Kulik HJ (2020) Large-Scale Comparison of 3d and 4d Transition Metal Complexes Illuminates the Reduced Effect of Exchange on Second-Row Spin-State Energetics. Physical Chemistry Chemical Physics 22 (34):19326-19341. doi:10.1039/d0cp02977g
118. Latimer AA, Kakekhani A, Kulkarni AR, Nørskov JK (2018) Direct Methane to Methanol: The Selectivity–Conversion Limit and Design Strategies. ACS Catalysis 8 (8):6894-6907. doi:10.1021/acscatal.8b00220
119. Bowman DN, Jakubikova E (2012) Low-Spin versus High-Spin Ground State in Pseudo-Octahedral Iron Complexes. Inorg Chem 51 (11):6011-6019
120. Kepp KP (2016) Theoretical Study of Spin Crossover in 30 Iron Complexes. Inorg Chem 55 (6):2717-2727